A global aerosol model forecast for the ACE-Asia field experiment

Mian Chin,[1,2] Paul Ginoux,[1,2,3] Robert Lucchesi [4,5]

[1] School of Earth and Atmospheric Sciences, Georgia Institute of Technology, Atlanta, GA

[2] Atmospheric Chemistry and Dynamics Branch, NASA Goddard Space Flight Center, Greenbelt, MD

[3] Current address: University of Maryland at Baltimore County, Baltimore, MD

[4] Data Assimilation Office, NASA Goddard Space Flight Center, Greenbelt, MD

[5] Science Applications International Corporation, Beltsville, MD

Submitted to the Journal of Geophysical Research – Atmospheres

ACE-Asia Special Issue – A

November 25, 2002

Abstract

We present the results of aerosol forecast during the ACE-Asia field experiment in spring 2001, using the Georgia Tech/Goddard Global Ozone Chemistry Aerosol Radiation and Transport (GOCART) model and the meteorological forecast fields from the Goddard Earth Observing System Data Assimilation System (GEOS DAS). The aerosol model forecast provides direct information on aerosol optical thickness and concentrations that were measured in the experiment, making flight planning more effective; while quick feedback from measurements helps improve the model processes, ensuring meaningful data analysis. During spring 2001, large amounts of pollution and dust aerosols originating in Asia were frequently transported to the Yellow Sea and the Sea of Japan. Several large dust outbreak episodes that allowed dust plumes to make their way across the Pacific to reach North America were all predicted by the model. Both the model forecast and the measurements showed that most pollution aerosols over the ACE-Asia measurement area were concentrated below 2 km, with sulfate as the dominant aerosol type. However, above 2 km, dust controlled the total aerosol optical thickness. The two pivotal elements in a successful aerosol model forecast operation are correct source locations that determine where the emissions take place, and realistic forecast winds and convection that decide where the aerosols are transported. Although the relatively coarse model grid resolution has limited our ability to resolve the detailed structure of the aerosols distributions as seen from the observations, our global model can effectively account for both the inflow and outflow of aerosols over the Asian-Pacific domain, keep track of the long-range transport and destination of the aerosol plumes, and coordinate experiments that are taking place at different geographic locations.

1. Introduction

The Asian Pacific Regional Aerosol Characterization Experiment (ACE-Asia), which took place during the spring of 2001 over the Asian-Pacific region, was designed to investigate the aerosol properties and their radiative forcing in the anthropogenically modified atmosphere of eastern Asia and northwestern Pacific. The intensive field study (3/30/2001 – 5/4/2001) of the ACE-Asia was concentrated over the Yellow Sea and the Sea of Japan and involved measurements from several aircraft and ships that were coordinated with the surface network and satellite observations to sample the Asian outflow [Huebert et al., this issue].

East Asia is an important source region of all major tropospheric aerosol types. It has been estimated that fast economic development, large areas of desert, and the intensive forest and agriculture fires in the region contribute to 1/4 to 1/3 of global emissions of SO_2, organic matter, soot, and dust [e.g. Chin et al. 2000, Chin et al. 2002; Ginoux et al. 2001; and references therein]. During the spring, the transport of airmass from the Asian continent to the western Pacific is at its maximum and, as a result, sources of anthropogenic and natural aerosols over Asia have a maximum impact on the Pacific and downwind regions. Depending on meteorological conditions such as wind direction, convection intensity, cloud coverage, and precipitation, the composition of aerosols over the ACE-Asia experiment area is either a mixture composed of multi-component aerosols, or dominated by one specific type of aerosol. In addition, long-range transport from Europe, Africa, and western Asia would add to the complexity of aerosol distributions and compositions over the western Pacific. A successful field experiment depends on careful daily planning, which requires the mission scientists to make optimal decisions based on the best available information.

This paper summarizes results of our modeling activity during the ACE-Asia using the Georgia Tech/Goddard Global Ozone Chemistry Aerosol Radiation and Transport (GOCART) model. During the intensive field study period indicated above, we used the GOCART model to provide a 24- to 96-hour forecast of aerosols everyday, and worked with the mission scientists and measurement teams on daily flight planning at the field operation center. Included in the products are horizontal and vertical distributions of aerosol composition, extinction, and optical thickness of sulfate, dust, black carbon (BC), organic carbon (OC), and sea-salt aerosols. The participation of a model in field experiments has two clear advantages. First, the aerosol forecast from the model provides direct information to mission scientists and measurement teams as to what should be expected on the amount, type, and distribution of aerosols as well as the duration of large episodes such as dust storms, information that is not readily available from the meteorological forecasts traditionally used in previous field programs. Second, the measurements provide feedback to the model as an instantaneous evaluation on the processes, such as sources and transport, dealt with in the model, thus constantly improving the model. Close interaction between the model and measurements established during the ACE-Asia has made the post-mission data analysis more fruitful.

While our extensive post-mission modeling and analysis of the ACE-Asia data will be elaborated on in several manuscripts in the next ACE-Asia special issue and elsewhere, we will here focus on the model forecasting and interaction with the measurements during the ACE-Asia field experiment. We will begin by describing the GOCART aerosol forecast processes (section 2) during the ACE-Asia 2001 fieldwork. We will then show the model forecast products and demonstrate how the measurements help improve the model (section 3). After discussing the strengths and limitations of the model (section 4), we will present our conclusions (section 5).

2. Aerosol forecast process

2.1. The GOCART model

Aerosol simulations in the GOCART model include major tropospheric aerosol types of sulfate, dust, OC, BC, and sea-salt (for detailed description of the model components, see Chin et al. 2000a, b; Ginoux et al. 2001; Chin et al. 2002). The model uses assimilated meteorological fields from the Goddard Earth Observing System Data Assimilation System (GEOS DAS), containing winds, temperature, pressure, specific and relative humidity, cloud mass flux, cloud fraction, precipitation, boundary layer depth, surface winds, and surface wetness. Physical processes in the model are emission, advection, convection, boundary layer mixing, wet deposition (rainout and washout), dry deposition, and settling. Chemical processes contain gas and aqueous phase reactions that convert sulfate precursors (dimethylsulfide and SO_2) to sulfate. A dust source parameterization has been constructed in the GOCART model, where locations of the dust sources are determined at the topographic depression areas with bare soil surface, while the dust uplifting probability is defined according to the degree of depression. The model simulation of dust aerosol has been found to be consistent with surface, lidar, and satellite observations [Ginoux et al. 2001]. The biomass burning emissions of BC and OC are based on the burned biomass inventory which is estimated using the satellite observations of fire counts and aerosol index [Duncan et al. 2002]. The new biomass burning emissions have since significantly improved the modeled seasonal variations of biomass burning and have made interannual biomass burning simulation possible [Chin et al. 2002].

The aerosol optical thickness is calculated from the mass concentrations, size distributions, refractive indices, and hygroscopic properties of individual type of aerosols. Discrete size bins of dust and sea salt are assumed with dry particle radii from 0.1 to 6 μm. We also assume

lognormal size distributions for sulfate, OC, and BC aerosols with effective dry radii of 0.16, 0.09, and 0.04 μm, respectively. The wavelength-dependent refractive indices are based on the Global Aerosol Data Set (GADS) [Köpke et al. 1997]. With the exception of dust, aerosols are considered to have different degrees of hygroscopic growth rate with ambient moisture. The hygroscopic growth factors are based on the GADS data and others [d'Almeida et al, 1991]. For example, at ambient relative humidity of 80%, the radius of wet sulfate, OC, BC, and sea-salt aerosols are a factor of 1.6, 1.5, 1.2, and 2 larger than their dry size (details of aerosol optical parameters and the calculation of optical thickness in the GOCART model have been provided in Chin et al. 2002).

2.2. GEOS DAS meteorological products

The meteorological data used to run the GOCART model are generated by the GEOS DAS, which is developed and run operationally by the NASA Goddard Data Assimilation Office (DAO). The GEOS DAS version 3 (GEOS-3) products were used in the model during the 2001 ACE-Asia field experiment. The GEOS-3 system is run by the DAO in two assimilation modes: the First Look assimilation and the Late Look assimilation. The First Look runs 4 times/day, about 8-15 hours behind real time, analyzing meteorological input data from conventional and satellite observations available at the time. The input data include upper air winds, geopotential heights, pressure, total precipitable water, sea-surface winds, sea-surface temperature, and sea-surface ice. The Late Look system configuration is similar to that for the First Look but it runs 2 to 3 weeks behind real time, allowing a more complete set of input observations to be integrated into the assimilation system. The First Look system also produces 5-day (0 – 120-hour) forecast products twice a day initialized at 0 and 12 hours of Universal Time (UT). The forecast products

are generated from the same GCM that is used in the assimilation, except that there is no observation data input to the system. The forecast system is initialized by the First Look assimilation output and runs 5 days forward. Table 1 lists the GEOS-3 prognostic and diagnostic fields used in our aerosol forecast and simulations.

2.3. Aerosol forecast

During the ACE-Asia period, we used the GEOS-3 First Look assimilation products to initialize the GOCART model and the 0 UT forecast products to generate aerosol forecast products. The DAO provided the forecast products at 2°x 2.5° horizontal resolution, while the assimilated products were at 1°x1°. We have regridded the 1°x 1° assimilated GEOS-3 data to 2°x 2.5° grid in order to obtain a consistent resolution and reduce the computational time. The vertical resolution in the original GEOS-3 data contains 48 sigma layers, with 22 layers above 30 mb. We aggregated the top 22 layers into 4 to reduce the total number of layers to 30 in our tropospheric simulations. The model layer thickness increases gradually from surface to the model top. Below 3 km, the vertical resolution varies from 24 m to 900 m. Above 3 km, the vertical resolution changes from 1 km to about 1.5 km near the tropopause.

Our daily forecast procedure involved processing the GEOS-3 data, running the GOCART forecast model, generating figures and animation, providing results on the website as well as to the Joint Office of Science Support (JOSS) field catalog for easy access from the operation field, and briefing the science team in the operation center for flight planning. The daily operation procedure is illustrated in Figure 1, and our 24 – 96-hour forecast products provided for the field operation are listed in Table 2. Since the local time at the ACE-Asia operation center in Japan

was 9 hours ahead of the UT, the first day (< 24 hours) forecast products were not relevant and thus not included in the standard forecast products and the JOSS field catalog.

Emissions in our forecast mode were basically the same as described in Chin et al. 2002. Anthropogenic emissions of SO_2 were taken from the Emission Database for Global Atmospheric Research [Olivier et al. 1996], and those of BC and OC were from a global dataset [Cooke et al., 1999]. We used the climatological biomass burning emissions of BC, OC, and SO_2 for March, April, and May, and only considered the continuously erupting volcanic emissions. Dust and sea salt emissions are calculated as a function of surface type and wind speed [Ginoux et al. 2001; Chin et al. 2002]. Updated emissions from sporadically erupting volcanoes, biomass burning, and anthropogenic sources are incorporated in the analysis mode as the information has become available after the field operation. Dust emissions in the analysis mode are also modified based on the information from the ACE-Asia measurements (see next section). These updated emissions are being used in our analysis mode, hence not discussed here. Figure 2 shows the emissions for April 2001 for sulfur (SO_2 and DMS), carbonaceous aerosols (BC + OC), dust, and sea salt used in our forecast mode.

3. Results

In this section we present the aerosol model forecast results that were used during the ACE-Asia to help plan the measurements, and the feedback from the measurements that was used to improve the model. A major advantage of 3-D model aerosol forecasting during the ACE-Asia field operation is its capability of making available the direct information of distributions, levels, and the evolution of aerosol species that were being measured in the experiment. This capability is especially important for ACE-Asia since the distribution of aerosols shows a very high spatial and temporal heterogeneity. Figure 3 illustrates the 24-hour model forecast products of sulfate

and dust optical thickness for April 2 and April 12, 2001. On April 2 2001 (top row, Figure 3), the model indicated that both Yellow Sea and the Sea of Japan were to receive large amounts of pollution from China with a total sulfate AOT of 0.3-0.5. On the other hand, there were also dust aerosols over the same region but with much lower AOT values. The NCAR C-130 was coordinated with the TRACE-P P-3B flight over the Sea of Japan on the same day, where the observations were consistent with the model forecast. As predicted in the model, most aerosols during that day were located in the boundary layer. There was a major dust outbreak on April 6-9, 2001, mainly from the Gobi and Mongolia plateau, east of Taklimaken desert. The dust plume traveled across the North Pacific and eventually reached North America within a few days. Figure 3 (bottom row) shows the sulfate and dust distributions on April 12. The passage of a cold front through China on April 9 –11 swept the polluted air from eastern China to the sea, leaving eastern China relatively "pollution free" (sulfate AOT from 0.05 to 0.15) while causing a pollution band located along 135°E, a few thousands of km away from the coast. However, the same front brought a large dust plume with it, filling the eastern China and coastal regions with relatively heavy dust. This type of information, which is difficult to extract from the traditional weather forecast, made flight planning more "visible" and effective.

The evolution and trans-Pacific transport of dust are demonstrated in Figure 4. The model 24-hour forecast of dust aerosol optical thickness for April 8, 11, and 14 are plotted on left column with the GEOS-3 forecast wind vectors at 4 km superimposed to indicate the general transport direction. On April 8, 2001, dust emitted from the source region and was transported to the Yellow Sea and the Sea of Japan. At the same time, there was another branch of dust wrapping around a low-pressure system centered at 50°N, 125°E (top panel, left column in Figure 4). The prevailing NW winds over central China and SW winds near the east coast

switched the dust plume from west-east direction on April 8 to southwest-northeast direction on April 11, with dust plume penetrating to as far south as 20°N over eastern China (middle panel). The dust plume meandered in a wavy pattern across the Pacific Ocean. On April 14, the entire west coast of North America from 30°N to 60°N were heavily influenced by the dust from Asia (bottom panel), which was moving further toward the U.S. inland. To verify the model forecast of dust transport on a large spatial scale, we plot on the right column in Figure 4 the aerosol index (AI) from the satellite sensor of Total Ozone Mapping Spectrometer (TOMS) for the same days (TOMS local over passing time is at about 11:10 am). Although the TOMS AI is usually more sensitive to the absorbing aerosols at altitudes above 2 km than those below, and could well be distorted by the presence of clouds, it is an excellent indicator of the presence of absorbing aerosols, such as dust and black carbon [Hsu et al., 1996; Herman et al., 1997; Torres et al., 1998]. The TOMS AI in Figure 4 shows very similar patterns of aerosol plume evolution and the trans-Pacific transport as predicted by the model, proving that the GEOS-3 forecast winds are quite realistic. We shall point out here that our dust source has been improved considerably since the ACE-Asia forecast operation such that the corrected dust AOT is typically a factor of 2 higher than that shown here. We will discuss the dust source later in the text.

We have found that a consistent feature of aerosol vertical distribution over the Yellow Sea and the Sea of Japan during ACE-Asia was that the pollution aerosols (mainly sulfate) were mostly concentrated below 2 km, dominating the total AOT there, while dust aerosols became more important above 2 km, with the plume sometimes extending to 8 km. Figure 5 shows the April monthly averaged sulfate and dust vertical distributions over the Yellow Sea (top panel) and the Sea of Japan (bottom panel). This vertical distribution calculated from the model forecast was consistent with the aircraft observations [Anderson et al., this issue]. The difference

in the vertical profiles between the sulfate and dust can be explained by the difference in their source locations. The pollution sources were located near the coast (Figure 2), and the pollution aerosols were mainly being transported to the ocean via boundary layer advection. In contrast, dust sources are further inland, and the major dust source regions are located above 1 km above the sea level. To reach the Pacific Ocean, dust emitted from its inland source regions has to be uplifted above the boundary layer and transported out. Often during springtime, dust plumes can reach the jet stream, efficiently being transported across the Pacific Ocean [Ginoux et al., 2001].

Model participation in a field experiment has a unique opportunity of close and timely interaction with the measurements with quick feedback for model evaluation and improvement. For example, the model forecast for April 24, 2001 over the Yellow Sea (when the C-130 aircraft made a flight to the Yellow Sea) indicated that there would be very little dust under 2 km, and the dust peak was expected at about 5-6 km with a concentration of 20 $\mu g\ m^{-3}$. However, the C-130 encountered heavy dust loading below 2 km, which was a factor of 5 or more greater than model predicted peak values. This miss-forecast had led us to reexamine the processes in the model that determine the dust distributions. We started by looking into the possible "missing source" over Asia. In our model, the potential sources for dust uplifting was determined to be located in the topographically low areas with bare soil coverage [Ginoux et al., 2001], based on the surface topographic map and the 1987 AVHRR land cover data [DeFries and Townshend, 1994]. The dust source location and strength determined by this method have been shown to agree in general with the in-situ and remote sensing observations [Ginoux et al., 2001; Prospero et al, 2002]. However, the method does not take into account of the recent desertification areas induced by human activities. To test the possible impact of dust sources from the desertification regions, we have consulted maps on recent desertification areas from China [CCICCD, 1997],

and added additional source areas over the Inner Mongolia Province in China, east of 110°E (Figure 6). These areas have been suffering from overgrazing and drought in recent years. As a consequence, they have become "bare soil" instead of "grassland" classified in the 1987 AVHRR land cover map [DeFries and Townshend, 1994]. The additional sources made a significant difference in model calculated dust vertical distributions over the Yellow Sea, as dust emitted from this region is readily advected to the Yellow Sea, contributing mostly to the low altitude dust loading. The vertical profiles of dust concentrations over the Yellow Sea on April 24, 2001 with and without the modified dust emission are shown in Figure 7 (top panel). With the additional Inner Mongolia sources, higher concentrations (up to 140 $\mu g\ m^{-3}$) of dust appear below 2 km, consistent with the observations. Interestingly, when the C-130 flew to the same area over the Yellow Sea the next day (April 25), much lower dust concentrations were detected below 2 km (Figure 7, bottom panel), in sharp contrast to the previous day. We then examined the differences in meteorological conditions between April 24 and 25 from the model that may explain the observations, realizing that even though the potential dust sources were the same in these 2 days, the surface winds were stronger over the eastern Inner Mongolia on April 24 than on April 25, thus the higher dust emission. The wind direction near the surface over this source region on April 25 was also shifted more to the west, compared with the NW winds in the previous day (April 24) that efficiently moved the dust to the Yellow Sea.

4. Discussion

Chemistry transport models (CTM) have only recently become an integral part of field operations, and will no doubt play increasingly important roles in the future. Here, we would like to assess the strengths and limitations of CTM forecasts from our experience in the ACE-Asia field experiment.

As shown in the previous section, the most valuable contribution of a CTM forecast is that it offers direct information on quantities that are being measured, such as concentrations of individual aerosol species and precursor gases, extinctions and optical thickness of individual and total aerosols, vertical and horizontal distributions, and time variations of these species, thus making the daily flight planning much more efficient than it would have been using the traditional weather forecast alone. Meanwhile, quick feedback from measurements helps improve the model processes.

Due to operational constraints during the forecast, the model was not always updated with the best information, which may result in discrepancies between the forecast and actual measured values. The most important quality of model products during the field operation is the accuracy of predicted spatial and temporal distributions of the aerosols, which is critically dependant on the source locations and the forecast winds in the model. As demonstrated in Figure 7 and discussed in the previous section, only when the correct source locations were included was the model able to produce reasonable aerosol vertical distributions. The accuracy of absolute values of aerosol concentrations or optical thickness, however, is not as important as the spatial distribution during the field operation, although it is essential in the post-mission data analysis. An example in Figure 8 shows the model calculated dust event on April 8, 2001 (when most dust was emitted from the Gobi and Mongolia plateaus) from our post-mission analysis, compared with the plot in Figure 4 from the forecast mode. In the analysis calculation, we used the Late Look assimilation of the GEOS-3 meteorological fields, added the desertification dust source locations in the eastern Inner Mongolia in China (see previous section), and extended the maximum dust particle size from 6 μm during forecast to 10 μm. The post-mission simulation (Figure 8) shows a dust distribution pattern very similar to the forecast (Figure 4, top left panel),

but the dust AOT is typically 2 times higher from the analysis than that from the forecast. However, it was the forecast information of the dust outbreak and the heavy plume transported to the Yellow Sea that had guided the aircraft for measurements over the Yellow Sea in the next few days. On the other hand, post-mission analysis allows sufficient time to incorporate updated information into the model for quantitative comparisons and interpretation when the model's ability to reproduce the actual quantities is critical.

Because the GEOS-3 provided a 5-day meteorological forecast twice daily, we were able to generate a 4-day aerosol forecast every day (the first day was not considered because of the difference between the field local time and the UT). We found in the field that although the 24 and 48 hour forecast products were most frequently used, 72 and sometimes 96 hour forecast products were also useful in facilitating flight planning 2-3 days in advance for obtaining flight permission at certain locations.

Although the ACE-Asia intensive operation was conducted in a limited area over the Yellow Sea and the Sea of Japan within 20°N – 45°N and 124°E – 140°E domain, a global model displays clear advantages in supporting such a limited area field experiment. First, our global model takes into account the transport of species from outside of the Asian regional domain to the measurement area (thus more comprehensive forecast products). Our analysis has found that dust from Africa and pollution from Europe often made their ways into the Asia continent and western Pacific, contributing to the total aerosol loading over the Asia-Pacific region [Chin and Ginoux, 2002; Ginoux, manuscript in preparation]. Second, the model tracks the long-range transport of large aerosol plumes after they leave the source regions (thus the impact of regional sources on a larger scale). This is particularly relevant in springtime at mid-latitudes, when the prevailing westerly winds can effectively transport aerosols and pollutants from one continent to

another. As shown in Figure 4, Asian dust during the large outbreak episodes does make an impact of hemispheric scale. Third, a global model forecast is instrumental in coordinating field experiments simultaneously conducted in different geographic locations. For example, in April 2001, the Photochemical Ozone Budget of the eastern North Pacific Atmosphere-2 (PHOEBIA-2) field experiment on the west coast of the U.S. measured CO and aerosols that had significant fraction from long-range transport from Asia. The PHOEBIA-2 group also used our global forecast products (see Table 2) for ACE-Asia in their daily flight planning [D. Jaffe, University of Washington, personal communication, 2001], making their measurements in concert with ACE-Asia in assessing the intercontinental transport.

While in general our model forecast captured large spatial and temporal variations of aerosol distributions over the region, our relatively coarse spatial resolution (2° x 2.5°) has limited the model forecast's capability for detailed spatial gradient over a few hundreds of kilometer of the typical daily flight coverage area, which were within only a few model gridboxes. The same is true of the vertical resolution; during the ACE-Asia field operation, for example, the observations sometimes showed that there were very well defined, stratified aerosol layers in about 1 km apart vertically [e.g., Huebert et al., this issue], yet, because of our coarse model vertical resolution (0.8 to 1 km in the middle troposphere, see Figure 5), we were unable to resolve the fine structures of the aerosol layers. In the future, the greater computing power and speed and 1° or higher spatial resolution meteorological data should enable us to provide finer resolution forecast products. More immediately, however, one may use a nested fine grid regional domain within a coarse grid global model, which can produce fine structures within the focused domain while considering trans-continental boundary transport without expensive computing requirements.

5. Conclusions

We have used the GOCART model and the meteorological forecast fields from the GEOS DAS to provide aerosol forecast supporting the ACE-Asia field experiment in spring 2001. This type of forecast provides direct information on aerosol optical thickness and concentrations that are measured in the experiment, making flight planning more effective toward achieving mission objectives. Meanwhile, quick feedback from measurements constantly improves the model processes. Close interaction between the model and measurements is essential to the success of a critical mission such as the ACE-Asia.

We have found that during spring 2001, large amounts of pollution and dust aerosols originating in the Asian continent were frequently transported to the Yellow Sea and the Sea of Japan. Several large dust outbreaks that allowed dust plumes to cross the Pacific to reach North America were also all predicted by the model. The model indicates that most pollution aerosols over the ACE-Asia measurement area were located below 2 km, with sulfate as the dominant aerosol type. However, above 2 km, dust aerosol controlled the total aerosol optical thickness. The model predictions were consistent with field observations.

We have also found that because our model did not take into account the dust source over the recent desertification areas in Inner Mongolia Province in China, the model missed a large amount of low altitude dust over the Yellow Sea observed in one flight. We have since corrected the dust source locations over China in our model so that our post-mission data analyses have become more meaningful [results to be presented elsewhere].

The two key elements in a successful aerosol model forecast operation during a field mission are correct source locations that determine where the emissions take place, and realistic forecast winds and convection that decide where the aerosols are transported. In the forecast mode, the

correct forecast of spatial distribution pattern of aerosol (plume location and height) is more critical for field operation planning than the accuracy of the quantities, such as concentration or optical thickness.

We have determined that the advantage of a global model in supporting field experiments is its effectiveness in accounting for the inflow and outflow of aerosols over a particular domain, in keeping track of the long-range transport and destination of the aerosol plumes, and in coordinating experiments that are taking place at different geographic locations (e.g. at source and receptor regions such as Asia and North America). However, the relatively coarse spatial resolution in our model has hindered our ability to resolve the detailed structure of the horizontal gradient and stratified vertical layers of aerosols as seen from the observations, since a typical flight only crosses a few model gridboxes. Therefore, we suggest that it would be plausible to nest a high resolution limited-area model within a global model so that it can deal with large-scale transport and yet have a fine resolution in the experiment domain with reasonable computing resources.

Acknowledgement

This work was supported by the NASA Radiation Sciences Program and the NSF Atmospheric Chemistry Program. We thank Thomas Owens and Doug Collins at the Goddard Data Assimilation Office and SAIC for providing the GEOS-3 forecast products during the ACE-Asia field operation.

References

Anderson, T. L., S. J. Masonis, D. S. Covert, N. C. Ahlquist, S. G. Howell, A. D. Clarke, and C. S. McNaughon, Variability of aerosol optical properties derived from in-situ aircraft measurements during ACE-Asia, *J. Geophys. Res.*, this issue.

Chinese Committee for Implementation of the Convention to Combat Desertification (CCICCD) Report, Beijing, 1997.

Chin, M., R. B. Rood, S.-J. Lin, J.-F. Müller, and A. M. Thomspon, Atmospheric sulfur cycle in the global model GOCART: Model description and global properties, *J. Geophys. Res., 105*, 24,661-24,687, 2000a.

Chin, M., D. Savoie, B. J. Huebert, A. R. Bandy, D. C. Thornton, T. S. Bates, P. K. Quinn, E. S. Saltsman, and W. J. De Bruyn, Atmospheric sulfur cycle in the global model GOCART: Comparison with field observations and regional budgets, *J. Geophys. Res., 105*, 24,689-24,712, 2000b.

Chin, M., P. Ginoux, S. Kinne, O. Torres, B. N. Holben, B. N. Duncan, R. V. Martin, J. A. Logan, A. Higurashi, and T. Nakajima, Tropospheric aerosol optical thickness from the GOCART model and comparisons with satellite and sunphotometer measurements, *J. Atmos. Sci., 59*, 461-483, 2002.

Chin, M., and P. Ginoux, From regional emissions to global atmospheric change: Intercontinental transport of aerosols in the context of ACE-Asia, paper presented at the IGAC 2002 Conference, Crete, Greece, September 2002.

Cooke, W. F., C. Liousse, H. Cachier, and J. Feichter, Construction of a 1x1 fossil fuel emissions data set for carbonaceous aerosol and implementation and radiative impact in the ECHAM4 model, *J. Geophys. Res., 104*, 22,137-22,162, 1999.

d'Almeida, G. A., *Atmospheric Aerosols,* A. Deepak publishing, 561 pp, 1991.

DeFries, R. S., and J. R. G. Townshend, NDVI-derived land cover classification at a global scale, *Int. J. Remote Sens., 15*, 3567-3586, 1994.

Duncan, B. N., R. V. Martin, A. C. Staudt, R. Yevich, and J. A. Logan, Interannual and seasonal variability of biomass burning emissions constrained by remote-sensed observations, *J. Geophys. Res.,* in press, 2002.

Ginoux, P., M. Chin, I. Tegen, J. Prospero, B. Holben, O. Dubovik, and S.-J. Lin, Sources and global distributions of dust aerosols simulated with the GOCART model, *J. Geophys. Res., 106*, 20,255-20,273, 2001.

Herman, J. R., P. K. Bhartia, O. Torres, C. Hsu, C. Seftor, and E. Celarier, Global distribution of UV-absorbing aerosols from Nimbus 7/TMOS data, *J. Geophys. Res.,102,* 16,991-16,922, 1997.

Hsu, N. C., J. R. Herman, P. K. Bhartia, C. J. Seftor, O. Torres, A. M. Thompson, J. F. Gleason, T. F. Eck, and B. N. Holben, Detection of biomass burning smoke from TOMS measurements, *Geophys. Res. Lett., 23*, 745-748, 1996.

Huebert, B., T. Bates, P. Russell, G. Shi, Y. J. Kim, and K. Kawamura, An overview of ACE-Asia: Strategies for quantifying the relationships between Asian aerosols and their climate impacts, *J. Geophys. Res.*, this issue.

Köpke, P., M. Hess, I. Schult, and E. P. Shettle, Global aerosol data set, Tech. Rep. 243, Max-Planck Institute, 44 pp., 1997.

Olivier, J. G. J., et al, Description of EDGAR version 2.0: A set of global emission inventories of greenhouse gases and ozone-depleting substances for all anthropogenic and most natural sources on a per contry bases and on 1x1 grid, RIVM/TNO Rep. 771060-002, 140 pp., 1996.

Prospero, J. M., P. Ginoux, O. Torres, S. Nicholson, and T. Gill, Environmental characterization of global sources of atmospheric soil dust identified with the NIMBUS 7 Total Ozone Mapping Spectrometer (TOMS) absorbing aerosol product, Rev. of Geosphys., 1002, 10.1029/2000RG000095, 2002.

Torres, O., P. K. Bhartia, J. R. Herman, Z. Ahmad, and J. Gleason, Derivation of aerosol properties from satellite measurements of backscattered ultraviolet radiation: Theoretical bases, *J. Geophys. Res., 103*, 17,099-17,110, 1998.

Table 1. GEOS-3 products used in the GOCART model.

Name	*Description*	*Dim*	*Time*	*Qty**
PS	Surface pressure (hPa)	2-D	3-hr	Inst
SLP	Sea level pressure (hPa)	2-D	3-hr	Inst
SURFTYPE	Surface types (water, land, ice, etc.)	2-D	3-hr	Inst
GWET	Soil moisture (% of field capacity)	2-D	3-hr	Inst
TROPP	Tropopause pressure (hPa)	2-D	3-hr	Inst
UWND	Zonal wind (m s^{-1})	3-D	6-hr	Inst
VWND	Meridional wind (m s^{-1})	3-D	6-hr	Inst
TMPU	Temperature (K)	3-D	6-hr	Inst
SPHU	Specific humidity (g kg^{-1})	3-D	6-hr	Inst
PREACC	Total precipitation (mm day^{-1})	2-D	3-hr	Avg
PRECON	Convective precipitation (mm day^{-1})	2-D	3-hr	Avg
HFLUX	Sensible heat flux (W/m^2)	2-D	3-hr	Avg
TGROUND	Ground temperature (SST over water) (K)	2-D	3-hr	Avg
RADSWG	Net downward shortwave flux at ground (W m^{-2})	2-D	3-hr	Avg
ALBEDO	Surface albedo (0-1)	2-D	3-hr	Avg
USTAR	Friction velocity (m s^{-1})	2-D	3-hr	Avg
Z0	Surface roughness (m)	2-D	3-hr	Avg
PBL	Planetary boundary layer depth (hPa)	2-D	3-hr	Avg
U10M	Zonal wind at 10 meters (m s^{-1})	2-D	3-hr	Avg
V10M	Meridional wind at 10 meters (m s^{-1})	2-D	3-hr	Avg
TAUCLD	Cloud optical depth	3-D	6-hr	Avg
CLDTOT	Cloud fraction	3-D	6-hr	Avg
CLDRAS	Convective cloud fraction	3-D	6-hr	Avg
MOISTQ	Specific humidity tendency, moist (g kg^{-1} day^{-1})	3-D	6-hr	Avg
DQLS	Specific humidity tendency, stratform (g kg^{-1} day^{-1})	3-D	6-hr	Avg
KH	Eddy diffusivity coefficient, scalars (m^2 s^{-1})	3-D	6-hr	Avg
CLDMAS	Cloud mass flux (kg m^{-2} s^{-1})	3-D	6-hr	Avg
DTRAIN	Detrainment cloud mass flux (kg m^{-2} s^{-1})	3-D	6-hr	Avg

*Quantity: Inst = instantaneous, Avg = average.

Table 2. GOCART model forecast products.

Forecast product	*Forecast frequency*
Latitude-longitude distributions:	
Optical thickness of individual and total aerosols	3 hour
Column burden (g m^{-2}) of individual aerosol species	3 hour
Latitudinal cross section at 125 °E, 135 °E, and 140 °E:	
Total Aerosol extinction (km^{-1})	3 hour
Individual aerosol concentration (g m^{-3})	3 hour
Longitudinal cross section at 30 °N and 40 °N:	
Total Aerosol extinction (km^{-1})	3 hour
Individual aerosol concentration (g m^{-3})	3 hour
Meteorological variables (GEOS DAS):	
Low level (700 – 1000 mb), mid-level (400 – 700 mb), and high level (above 400 mb) cloud cover	3 hour
Total precipitation (mm day^{-1})	3 hour
Wind speed and direction at 0.1 km and 4 km	6 hour
Global distributions:	
Optical thickness for individual and total aerosols	3 hour
Concentration of sulfate and dust at 0.1, 4, and 6 km	3 hour

Figure Captions

Figure 1. Schematic of the GOCART model forecast process during ACE-Asia.

Figure 2. Emissions of aerosols and precursor gases in April 2001 used in the GOCART forecast mode: (a) sulfur (DMS + SO_2), (b) carbonaceous (BC + OC), (c) dust, and (d) sea-salt.

Figure 3. The GOCART model aerosol forecast of sulfate (left column) and dust (right column) AOT at 500 nm on April 2 (top row) and April 12 (bottom row), 2001.

Figure 4. The GOCART model forecast of dust evolution and trans-Pacific transport (shown as AOT, left column) and TOMS AI (right column) on April 8 (top row), April 11 (middle row), and April 14 (bottom row), 2001.

Figure 5. Model calculated monthly averaged vertical profiles of sulfate (circles and line) and dust (stars and line) in April 2001 over the ACE-Asia flight areas of the Yellow Sea (121°E – 126°E, 30°N – 36°N, top panel) and the Sea of Japan (130°E – 138°E, 36°N – 40°N, bottom panel). Symbols are at the centers of the model layers.

Figure 6. Dust emission in April 2001 after adding the desertification sources in the Inner Mongolia Province and extended dust particle size to 10 μm (compared to Figure 2c).

Figure 7. Vertical profiles of dust over the Yellow Sea on April 24 (top)and April 25 (bottom), 2001. Dashed lines are the model forecast results with dust emissions in Figure 2c, and solid lines are the model analysis results with additional sources over the Inner Mongolia Province in Figure 6.

Figure 8. The GOCART model simulated dust AOT for April 8, 2001 using the GEOS-3 Late Look assimilated meteorological fields and updated dust sources (compared to Figure 4, see text for details).

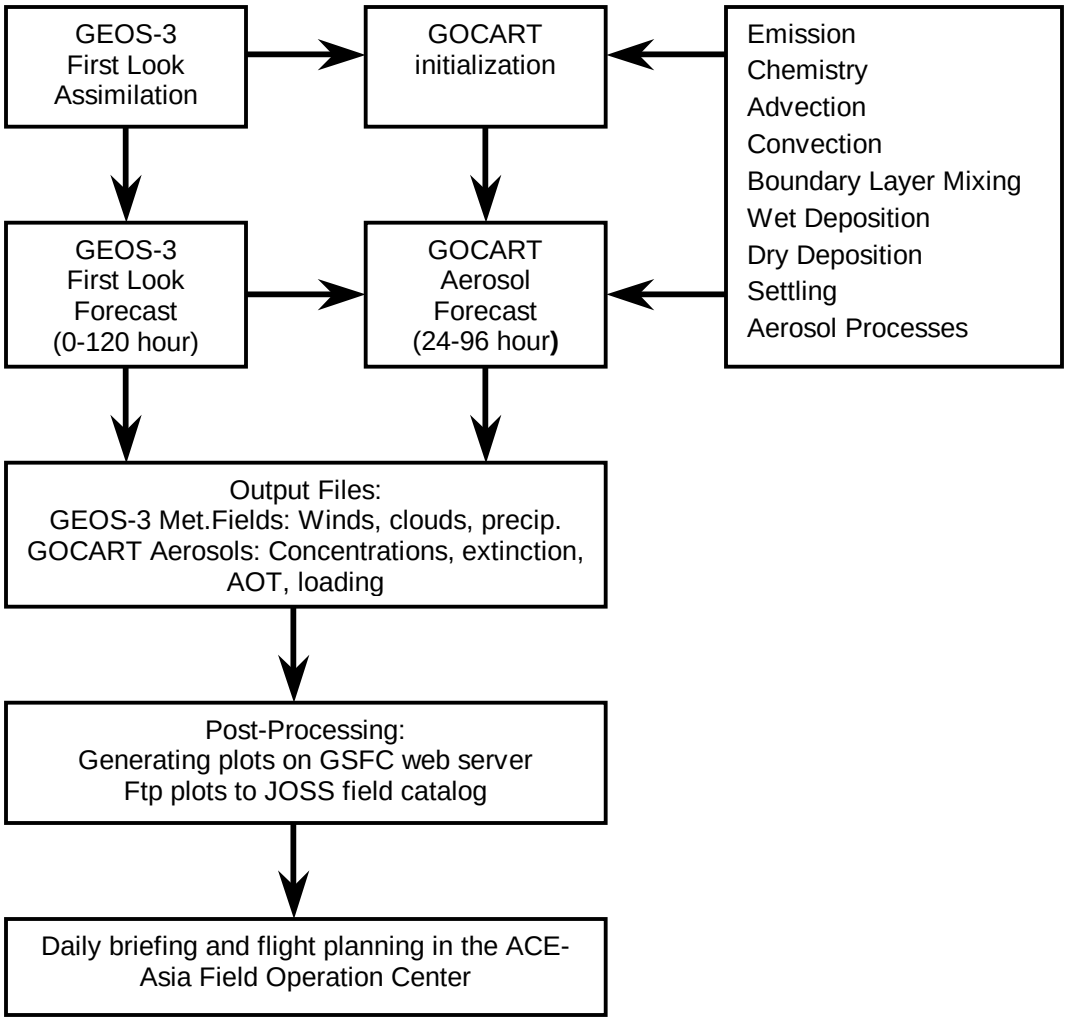

Figure 1. Schematic of the GOCART model forecast process during ACE-Asia.

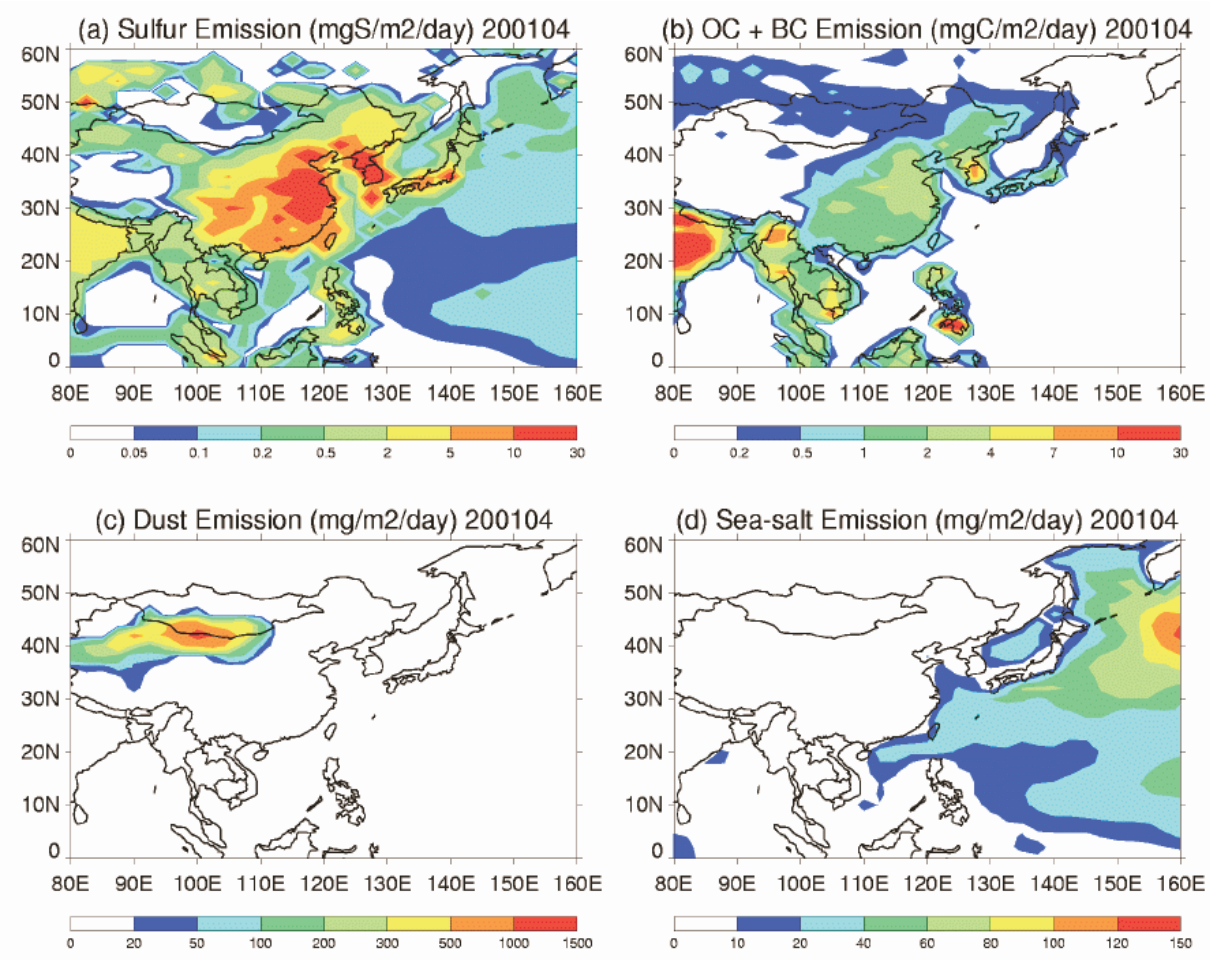

Figure 2. Emissions of aerosols and precursor gases in April 2001 used in the GOCART forecast mode: (a) sulfur (DMS + SO_2), (b) carbonaceous (BC + OC), (c) dust, and (d) sea-salt.

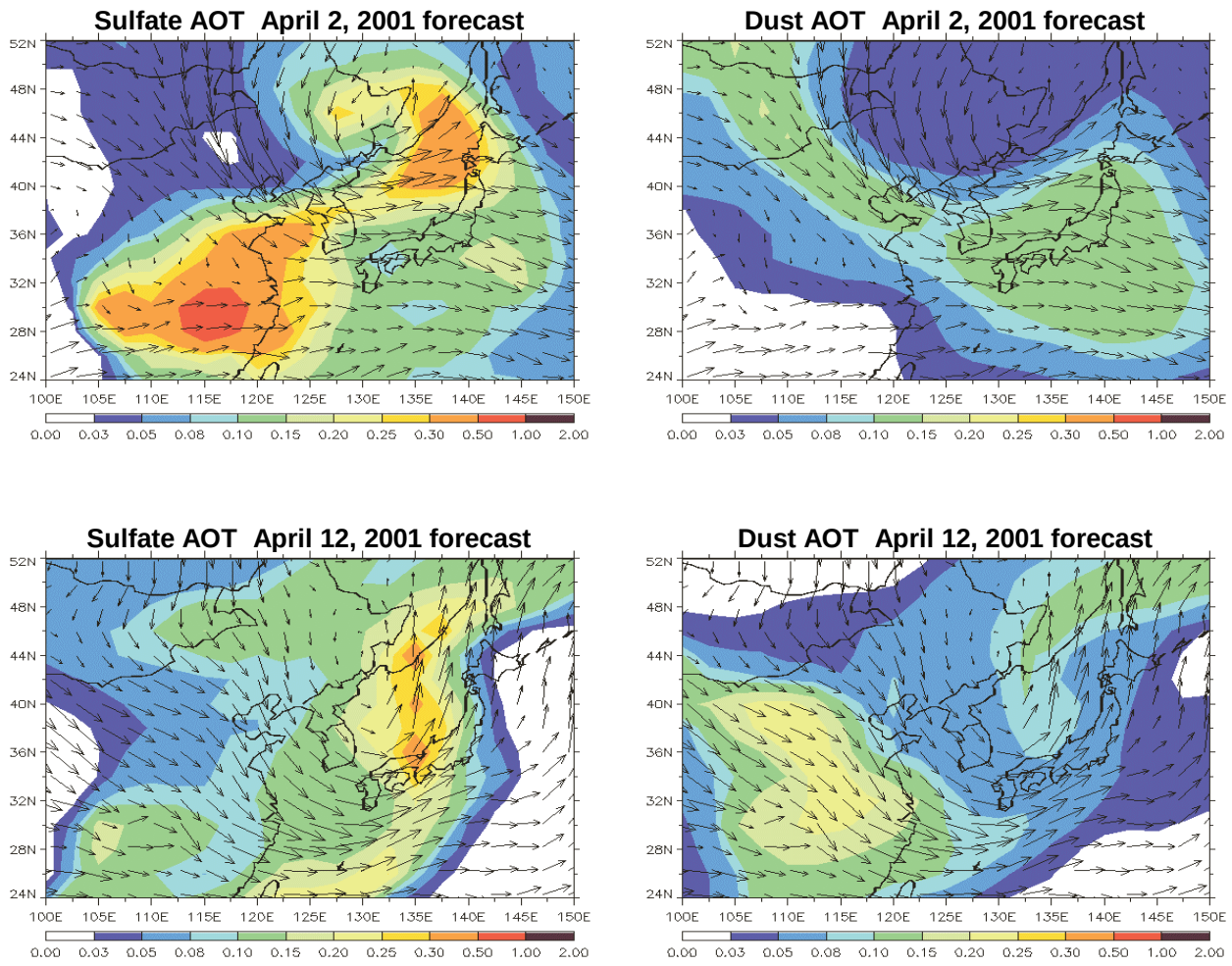

Figure 3. The GOCART model aerosol forecast of sulfate (left column) and dust (right column) AOT at 500 nm on April 2 (top row) and April 12 (bottom row), 2001.

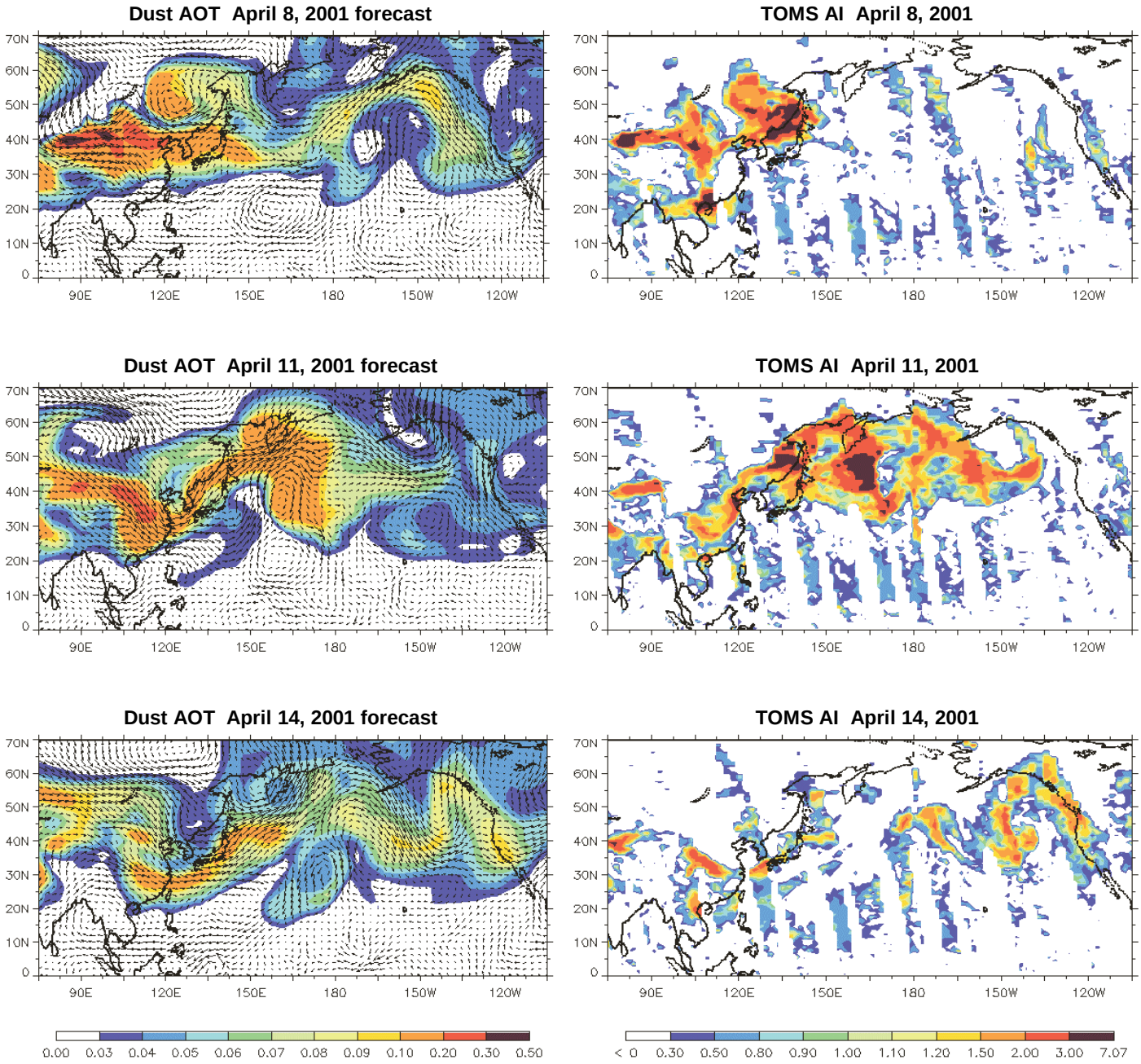

Figure 4. The GOCART model forecast of dust evolution and trans-Pacific transport (shown as AOT, left column) and TOMS AI (right column) on April 8 (top row), April 11 (middle row), and April 14 (bottom row), 2001.

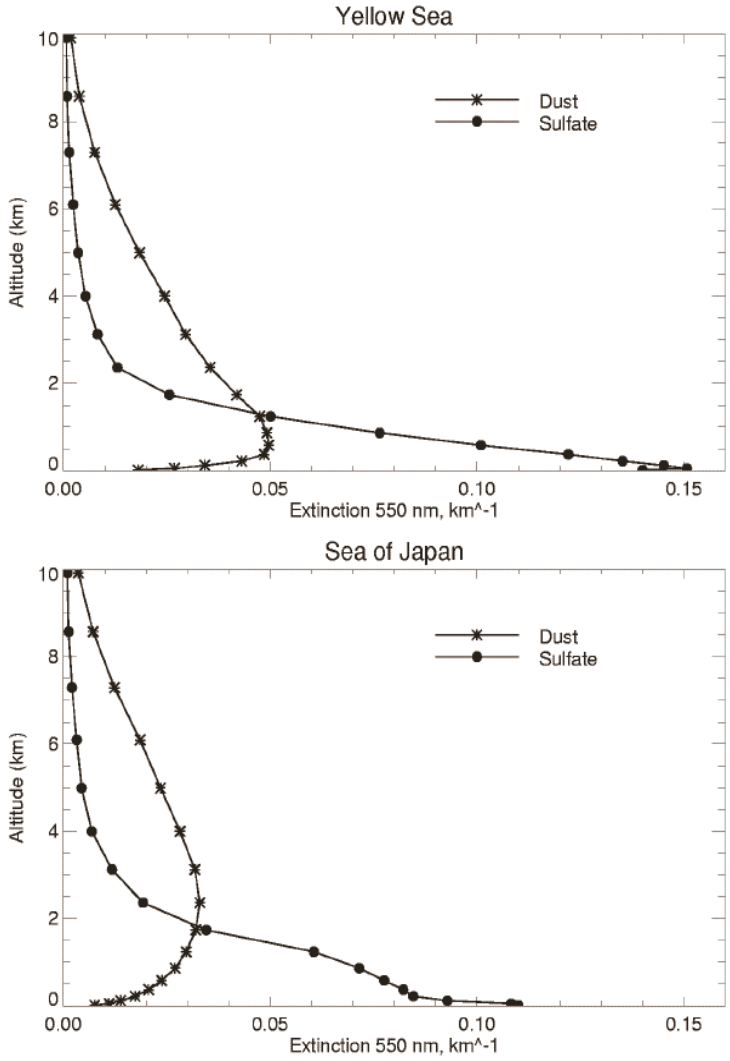

Figure 5. Monthly averaged vertical profiles of sulfate (circles and line) and dust (stars and line) in April 2001 over the ACE-Asia flight areas of the Yellow Sea (121°E – 126°E, 30°N – 36°N, top panel) and the Sea of Japan (130°E – 138°E, 36°N – 40°N, bottom panel). Symbols are at the centers of the model lavers.

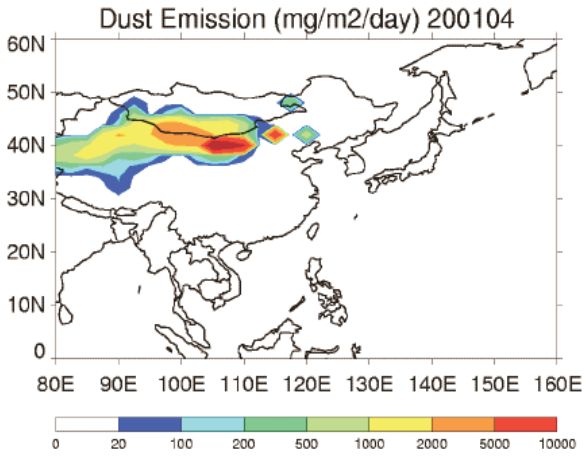

Figure 6. Dust emission in April 2001 after adding the desertification sources in the Inner Mongolia Province and extended dust particle size to 10 μm (compared to Figure 2c).

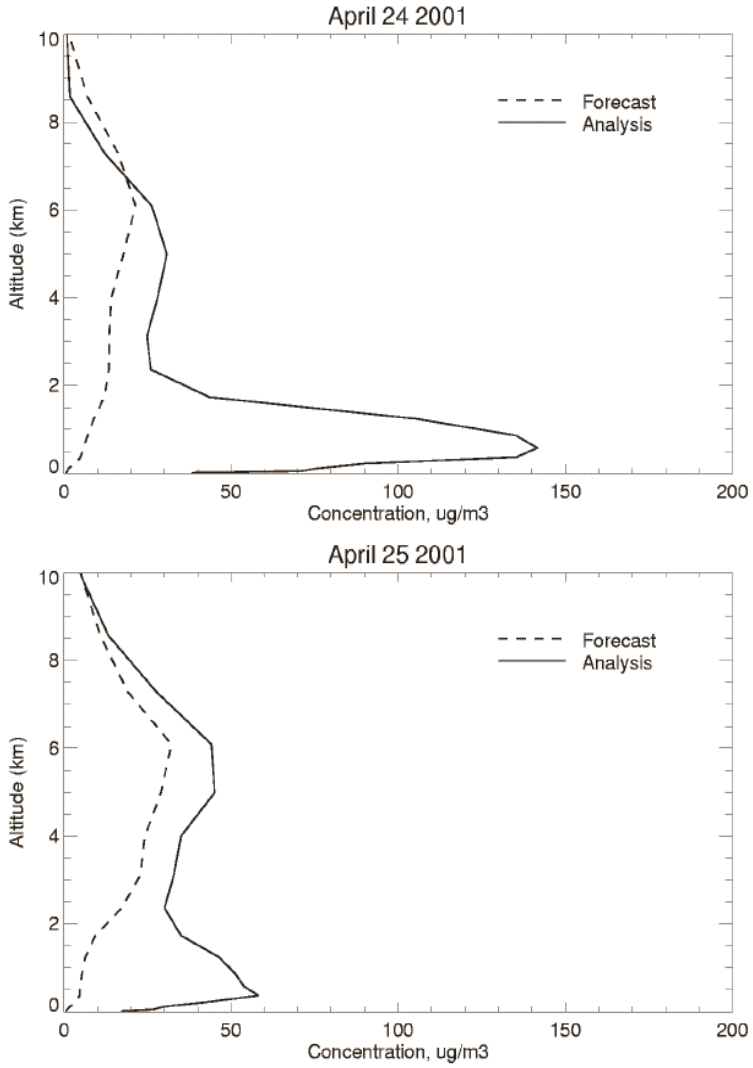

Figure 7. Vertical profiles of dust over the Yellow Sea on April 24 (top panel) and April 25 (bottom panel), 2001. Dashed lines are the model forecast results with dust emissions in Figure 2c, and solid lines are the model analysis results with additional sources over the Inner Mongolia Province in Figure 6.

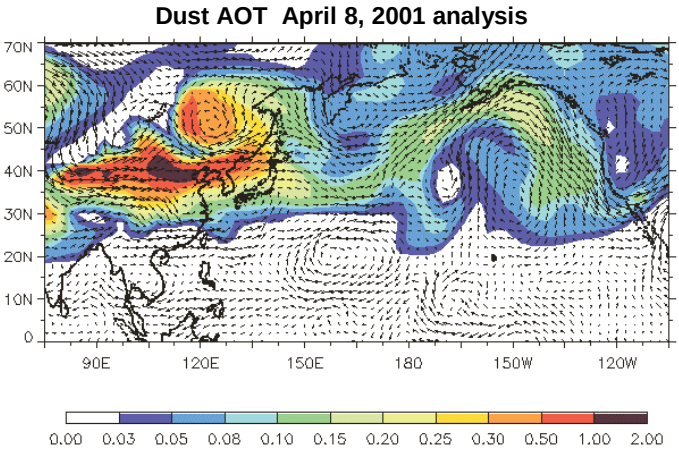

Figure 8. The GOCART model simulated dust AOT for April 8, 2001 using the GEOS-3 Late Look assimilated meteorological fields and updated dust sources (see text for details).